

# Mass of particles released by comet 12P/Pons-Brooks during 2023-2024 outbursts

Maria Gritsevich,<sup>1,2,3\*</sup> Marcin Wesołowski,<sup>4†</sup> Alberto J. Castro-Tirado<sup>5,6‡</sup>

<sup>1</sup>*Faculty of Science, University of Helsinki, Gustaf Hallströmin katu 2, FI-00014 Helsinki, Finland*

<sup>2</sup>*Swedish Institute of Space Physics (IRF), Bengt Hultqvists väg 1, 981 92 Kiruna, Sweden*

<sup>3</sup>*Institute of Physics and Technology, Ural Federal University, Mira str. 19, 620002 Ekaterinburg*

<sup>4</sup>*University of Rzeszów, Faculty of Exact and Technical Sciences, Institute of Physics, Pigońia 1 Street, 35-310 Rzeszów, Poland*

<sup>5</sup>*Instituto de Astrofísica de Andalucía (IAA-CSIC), Glorieta de la Astronomía s/n, E-18008, Granada, Spain*

<sup>6</sup>*Ingeniería de Sistemas y Automática, Universidad de Málaga, Unidad Asociada al CSIC por el IAA, Escuela de Ingenierías Industriales, Arquitecto Francisco Peñalosa, 6, Campanillas, 29071 Málaga, Spain*

Accepted XXX. Received YYY; in original form ZZZ

## ABSTRACT

During its most recent return, comet 12P/Pons-Brooks experienced 14 well-documented outbursts, observed between June 13, 2023, and April 2024, at heliocentric distances ranging from 4.26 au to 0.85 au. After perihelion, two additional outbursts were observed in summer 2024, at heliocentric distances of 1.20 au and 2.26 au. Using observational data, we developed a numerical model to estimate the mass ejected during these events, focusing on the sublimation of ice through the porous cometary nucleus. The key factors affecting ejected mass estimates are the outburst amplitude and the active surface area during both quiet sublimation and the outburst phases. Pogson’s law was used to express outburst magnitude, incorporating scattering cross-sections of cometary agglomerates. The model iteratively determined the mass ejected in observed outbursts, considering various ice types (H<sub>2</sub>O and CO<sub>2</sub>) controlling sublimation activity. Our results indicate that the mass ejected during these outbursts ranged from 10<sup>10</sup> to 10<sup>13</sup> kg. Our findings highlight the significant role of surface morphology and thermodynamic conditions in cometary outbursts, providing insights into the mechanisms driving these phenomena and their implications for cometary evolution and dust trail formation. Based on the analysis of observational data, we propose a six-level classification scheme for cometary outbursts.

**Key words:** comets: general – comets: individual: 12P/Pons-Brooks – Scattering – Meteoroid

## 1 INTRODUCTION

Occasionally, comets undergo sudden and intense surges in brightness and activity, a phenomenon referred to as cometary outbursts. These events involve the rapid release of significant amounts of gas and dust from the nucleus, temporarily amplifying the comet’s brightness and apparent size. Cometary outbursts offer a glimpse into the broader context of cosmic evolution. Direct observations reveal these phenomena as spectacular, involving a sudden increase in brightness by at least 1 magnitude. While astronomical data show a wide range of brightness changes in comets, from numerous mini outbursts as seen with comet 67P/Churyumov-Gerasimenko during the *Rosetta* mission (Vincent et al. 2016) to larger amplitude events like those exhibited by comets 1P/Halley (West et al. 1991), 174P/Echeclus (Skiff 2018), and 29P/Schwassmann-Wachmann (Miles 2016a), the fundamental problem of brightness change, often linked to the thermodynamic evolution of cometary nuclei under rapidly changing conditions, remains unresolved.

Despite extensive research, various mechanisms pro-

posed in the literature (Hughes 1990; Prialnik et al. 1995; Gronkowski and Wesołowski 2015; Miles 2016a,b; Wesołowski 2021; Wesołowski et al. 2022b; Guliev et al. 2022; Ye and Vaubaillon 2022; Belousov and Pavlov 2024a,b; Müller et al. 2024) have yet to fully elucidate the basic morphological features associated with cometary outbursts. These mechanisms typically involve the destruction of a fragment of the cometary surface, releasing substantial amounts of gas and dust from the nucleus into the coma. This outgassing process contributes to the density increase and expansion of the coma surrounding the nucleus, fundamentally altering the comet’s appearance and behavior. The expelled material, composed of volatile gases and dust particles, enhances sunlight scattering on porous dust-ice particles, leading to the characteristic appearance of a bright central nucleus surrounded by a diffuse coma (Fig. 1), resulting in overall increased comet brightness during an outburst (Wesołowski 2021; Gritsevich et al. 2022).

The ejection of dust particles and debris from a comet nucleus during outburst events is intricately linked to the formation of meteoroid streams. Appendix A of this paper presents an estimate of the size of particles ejected from the nucleus of comet 12P/Pons-Brooks, necessary for such calculations. Initially appearing to dissipate, these particles form a cloud that gradually expands, primarily influenced by solar radiation pressure and gravitational forces. After half a rev-

\* E-mail: maria.gritsevich@helsinki.fi

† E-mail: mwesolowski@ur.edu.pl

‡ E-mail: ajct@iaa.es

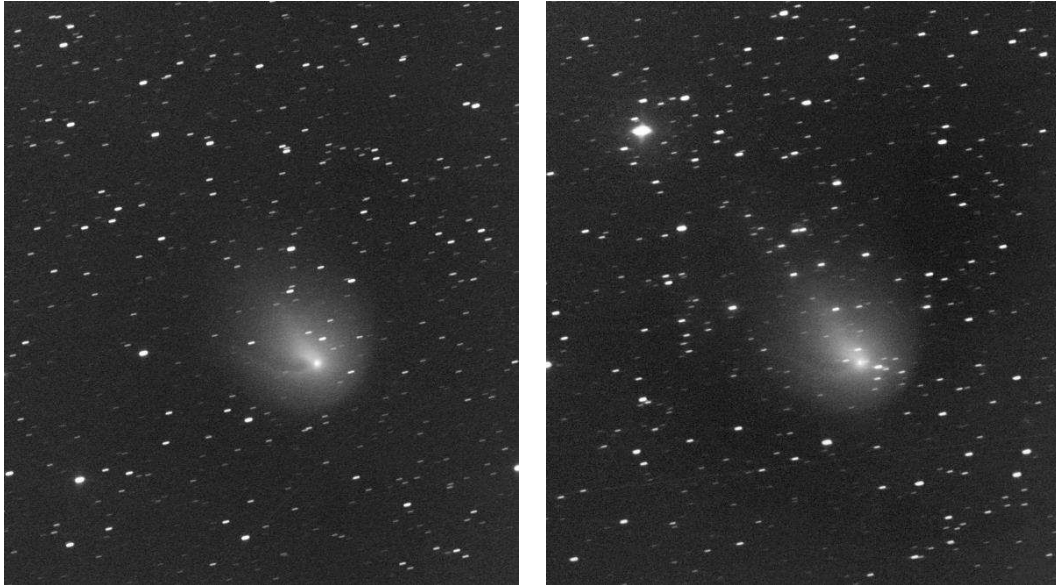


**Figure 1.** Outbursts of comet 12P/Pons-Brooks with a visible coma surrounding its nucleus. Both images were obtained remotely using a T21 0.43-m f/4.5 Corrected Dall-Kirkham astrograph and CCD camera at the iTelescope observatory (U94) in the Great Basin Desert, Beryl Junction, Utah, USA. The total brightness, nuclear brightness, and coma diameter were estimated separately for each date: 1) 2023 November 26.08 UT;  $m_1=8.9$  mag.,  $m_2=13.9$  mag., Dia.=5.1'; 2) 2023 November 27.08 UT;  $m_1=8.8$  mag.,  $m_2=13.9$  mag., Dia.=5.7'.

olution, the particles reconverge on the opposite side of the Sun near the mutual node of their orbits. Subsequent revolutions bring these particles back to their original outburst location [Lyytinen et al. \(2013\)](#); [Gritsevich et al. \(2022\)](#), forming an hourglass-shaped trail due to variations in particle orbits.

The formation of a meteoroid stream is a gradual process spanning multiple orbits of the comet, as its ejected particles follow their orbital trajectories. Over time, these streams can intersect the planetary atmospheres, including those of Earth or Venus, leading to observable meteor showers ([Christou 2010](#); [Christou and Gritsevich 2024](#)). An example of this phenomenon is seen in the connection between comet 12P/Pons-Brooks and the weak December  $\kappa$ -Draconids meteor shower, typically occurring from November 29 to December 13 ([Tomko and Neslušan 2016](#)).

12P/Pons-Brooks is a periodic comet with an orbital period of approximately 71 years and a nucleus radius of  $17\pm 6$  km ([Ye et al. 2020](#)). Assuming the density of the cometary nucleus of  $500 \text{ kg}\cdot\text{m}^{-3}$ , the approximate value of its mass can be estimated  $1.03\cdot 10^{16}$  kg. This comet is notable for its brightness, reaching an absolute visual magnitude of approximately 5 near perihelion. Initially discovered in July 1812 by Jean-Louis Pons at Marseilles Observatory, it was later observed during its next appearance in 1883 by William Robert Brooks ([Yeomans 1986](#)). Ancient records suggest previous apparitions of comet 12P/Pons-Brooks (hereinafter referred to as 12P). With advancements in observational technology over the past 70 years, the comet's most recent perihelion passage on April 21, 2024, and its closest approach to Earth at 1.55 au on June 2, 2024, have been extensively documented.

In this study, we investigate the initial phases of the well-documented outbursts of comet 12P by employing a numerical model that estimates the ejected mass. Our findings have broader implications for understanding comet behaviour and the formation of dust trails, aiding in predicting the evolution and future observability of such events. Additionally, based on observations, we have developed a classification of outbursts, detailed in section 5.

## 2 OBSERVATIONS OF COMET 12P/PONS-BROOKS

Astronomical observations of comet 12P during its latest return, spanning from the initial signs of activity on June 13, 2023, to April 2024, covered heliocentric distances ranging from 4.26 au to 0.85 au, and revealed a total of 14 outbursts. After perihelion, two more outbursts were documented at heliocentric distances of 1.20 au and 2.26 au. The facilities used in early observations included the BOOTES (Burst Observer and Optical Transient Exploring System) — a Global Network of Robotic Astronomical Observatories ([Castro-Tirado et al. 1999](#); [Castro-Tirado 2023](#)), the 0.3 m Viestikallio remote observatory in Finland, the remote 0.3 m Makroskooppi observatory in Spain, and remote telescopes at the iTelescope observatories in Utah and California ([Prystavski et al. 2024](#); [Trigo-Rodriguez et al. 2024](#); [Borderes-Motta et al. 2024](#); [Gritsevich et al. 2025a](#)). The expansion rates triggered by the approximately 5-magnitude outburst on 2023-10-05.16 ([Usher et al. 2023](#)) were earlier reported based on these observations and the initiation time of the outburst ([Ryske et al. 2023](#)). The complete list of instruments used for the observations in this study is presented in Tab.(1). Sample images of comet 12P are shown in Figs. 1 and 2; see also ([Gritsevich et al. 2025b](#)).

Observations of comet 12P continued into 2024, with several outbursts reported before the comet reached perihelion on April 21 and achieved its peak brightness. Despite the increasing brightness, observational conditions became increasingly challenging as the comet approached closer to the Sun. A final pre-perihelion observation was attempted on April 2. At that time, the comet was situated very low in the local evening twilight sky, with an altitude of  $+16^\circ$  and the Sun at an altitude of  $-12^\circ$ . The comet appeared bright, featuring a long ion tail extending toward the northeast, with a position angle of  $39^\circ$ . After perihelion, comet 12P/Pons-Brooks reached its closest approach to Earth on June 2, at a distance of 1.55 au, becoming more visible from the Southern Hemisphere ([Gritsevich et al. 2025b](#)).

**Table 1.** List of telescopes and cameras used in observations of comet 12P/Pons-Brooks.

No	Optical Design	Aperture [mm]	F/Ratio	CCD/CMOS	Sensor	Telescope	MPC code
1.	Hyperbolic Flat-Field Astrograph	250	f/3.4	SBIG ST-10XME	KAF3200E	T05	U94
2.	Corrected Dall-Kirkham Astrograph	610	f/6.5	FLI-PL09000	KAF-09000	T24	U69
3.	Corrected Dall-Kirkham Astrograph	510	f/4.5	FLI-PL11002M	KAI-11002	T11	U94
4.	Rowe Ackerman Schmidt Astrograph	279	f/2.2	ZWO ASI2600 Color	SONY IMX571	T68	U94
5.	Corrected Dall-Kirkham Astrograph	431	f/6.8	FLI-PL16803	KAF-16803	T19	U94
6.	Corrected Dall-Kirkham Astrograph	431	f/4.5	FLI-PL6303E	KAF-6303E	T21	U94
7.	Petzval Apochromat Astrograph	106	f/5.0	ZWO ASI2400C	Sony IMX410	T20	U94
8.	Newtonian	250	f/3.8	ASI6200 Pro Series	Sony IMX455	T75	X07



**Figure 2.** Color image of comet 12P/Pons-Brooks, showing the “dark lane” feature visible inside the coma, obtained on 2023 November 19.11 UT. The image was captured remotely using a T68 0.28-m f/2.2 RASA astrograph and CMOS camera at the iTelescope observatory (U94) in the Great Basin Desert, Beryl Junction, Utah, USA. The estimated total magnitude is 8.7, with a coma diameter of 9.1 arcmin. A faint tail, approximately 17.7 arcmin in length, is visible at a position angle of 44°.

### 3 METHODS

Based on the extensive observational data we utilize a numerical model to determine the mass ejected during these outbursts. The key parameter in this determination is the estimation of the ice sublimation flux occurring through the porous structure of the nucleus of comet 12P. Estimating the mass ejected as a result of an outburst is a complex problem that depends on many parameters. In this study, we rely on Pogson’s law, which can be defined as:

$$\Delta m = -2.512 \log \frac{p(\theta)_N A_N S_N + p(\theta)_2 (C(t_2) + C_{ej})}{p(\theta)_N A_N S_N + p(\theta)_1 C(t_1)}. \quad (1)$$

In Eq.1  $p(\theta)_1$  represents the phase function of the cometary nucleus,  $p(\theta)_2$  is the phase function of the cometary agglomerates,  $A_N$  is the albedo,  $S_N$  is the total area of the comet,  $C(t_1)$  is the scattering cross-section of the cometary agglomerates raised into a coma during the quiet sublimation phase ( $t_1$ ),  $C(t_2)$  is the scattering cross-section of the cometary agglomerates raised into a coma during the outburst phase ( $t_2$ ),  $C_{ej}$  is the scattering cross-section of agglomerates originating from the destroyed and ejected layer of the nucleus. The individual scattering cross-sections that appear in Eq.1 can be expressed as (Wesołowski 2022a):

$$C(t_1) = \eta_1 \xi \frac{\int_{r_{\min}}^{r_{\max}} Q_{\text{scat}}(r) r^{2-q} dr}{\int_{r_{\min}}^{r_{\max}} r^{3-q} dr}, \quad (2)$$

$$C(t_2) = (\eta_1 + \Delta\eta) \xi \frac{\int_{r_{\min}}^{r_{\max}} Q_{\text{scat}}(r) r^{2-q} dr}{\int_{r_{\min}}^{r_{\max}} r^{3-q} dr}, \quad (3)$$

and

$$C_{ej} = \frac{3M_{ej} \int_{r_{\min}}^{r_{\max}} Q_{\text{scat}}(r) r^{2-q} dr}{4\rho_{gr}(1-\psi) \int_{r_{\min}}^{r_{\max}} r^{3-q} dr}. \quad (4)$$

In Eqs.(2-4)  $\eta_1$  is the active surface during quiet sublimation,  $\Delta\eta$  is a correction related to the ejection of a fragment of the cometary nucleus surface during the outburst,  $\xi$  is a factor related to thermodynamic parameters,  $r$  is the radius of porous particles on which the incident sunlight scatters,  $Q_{\text{scat}}(r)$  is the scattering coefficient,  $q$  is an index in the power law,  $M_{ej}$  is the mass ejection,  $\rho_{gr}$  is the density of particles, and  $\psi$  is the porosity of particles. Eqs.(2-3) contain two parameters that can be expressed as:

$$\xi = \frac{3S_N \gamma_j \psi F_i R_c}{v_g \rho_{agg}}, \quad (5)$$

and

$$\Delta\eta = \frac{M_{ej}}{4S_N h \rho_{gr}(1-\psi)}. \quad (6)$$

In Eqs.(5-6)  $\gamma_j$  is the dust-gas mass ratio (if  $j = 1$  then comet activity occurs in the quiet sublimation phase and if  $j = 2$  then comet activity occurs in the outburst phase),  $F_i$  is the sublimation flux (if  $i=1$ , this sublimation activity is controlled by ice  $\text{H}_2\text{O}$ , and when  $i=2$ , this sublimation activity is controlled by ice  $\text{CO}_2$ ),  $R_c$  is radius of the cometary coma,  $\rho_{agg}$  is the density of agglomerates,  $v_g$  is the gas velocity, and  $h$  is the thickness of the destroyed layer. The parameter  $\eta(t_1)$  defines the fraction of the nucleus surface actively sublimating during periods of quiet activity, relative to its total surface area. In our calculations, we consider a broad range for this parameter, extending up to 50%, reflecting observations from comet 67P/Churyumov-Gerasimenko where water ice sublimation predominantly occurred



on sunlit areas of the nucleus (Gicquel et al. 2016). To determine the value of the mass expelled during the outburst, we also need to ascertain individual thermodynamic parameters such as gas velocity and sublimation flux. This requires resolving the energy balance equation, which can be represented as follows:

$$\frac{S_{\odot}(1 - A_N)}{r_h^2} \max(\cos \Theta_{\text{Sun}}, 0) = \epsilon \sigma_B T_i^4 + H_k F_i, \quad (7)$$

where  $S_{\odot}$  is the solar constant at 1 au,  $\Theta_{\text{Sun}}$  is the solar zenithal angle,  $r_h$  is the heliocentric distance at which the comet outburst was observed,  $\epsilon$  is the emissivity,  $\sigma_B$  is the Stefan Boltzmann constant,  $T$  is the temperature, and  $H_k$  is the latent heat of sublimation (if  $k=1$  then we take into account the latent heat of sublimation of ice  $\text{H}_2\text{O}$ , and if  $k=2$  then we take into account the latent heat of sublimation of ice  $\text{CO}_2$ ). Let us explain that correctly describing the sublimation of cometary ice is not a simple task. Using thermodynamic models, one can determine the temperature, but this requires adopting certain values in the model that are poorly defined. An example of such a parameter is the thermal conductivity of the surface layer of the core and the changes occurring in this layer under the influence of the sublimation flux. Therefore, in order not to underestimate or overestimate the temperature value due to the uncertainty of thermal conductivity in the energy balance equation, this factor was omitted.

Additionally, the gas velocity and sublimation flux are calculated using the following relationships:

$$v_g = \sqrt{\frac{\pi k_B T_i}{2m_{g,i}}}, \quad (8)$$

and

$$F_i = \beta \psi p_{\text{sat},i} \sqrt{\frac{\pi m_{g,i}}{2k_B T_i}}, \quad (9)$$

where  $k_B$  is the Boltzmann constant,  $m_{g,i}$  is the mass of a gas molecule,  $\beta$  is the sticking coefficient of the gas molecules on to the surface (the value of this coefficient is in the range  $0 < \beta < 1$ ), and  $p_{\text{sat},i}$  is the pressure of the phase equilibrium.

## 4 RESULTS

To determine the actual ejected mass responsible for the outburst, Eq.1 needs to be solved numerically. Put simply, we are seeking the mass ejected value corresponding to a specific outburst amplitude. Eq.1 is a complex logarithmic function of the individual scattering cross-sections. Hence, we utilized an algorithmic approach for numerical solution. This involved iteratively refining the mass ejected value until convergence criteria were met. In our context, this iterative process identifies the mass ejected value for the observed outburst occurring at a particular heliocentric distance.

The list of the most important physical constants used in the model is presented in Tab.(2). The calculation results of thermodynamic parameters and mass ejected for two example values of the  $\eta$  parameter are presented in Tab.(3). An example of a graphical interpretation of the mass ejected as a function of the  $\eta$  parameter for two extreme values of the outbursts of the comet 12P is presented in Fig.(3).

Considering the factors discussed above, we determined the number of particles on which the incident sunlight was scattered, causing the comet to outburst. Key considerations included the ejected mass, which correlates with the active surface area during quiet sublimation, and the power-law distribution used to estimate the average particle size within the coma (Wesołowski et al. 2022b). To illustrate the varying contributions of different cross-sections to the amplitude

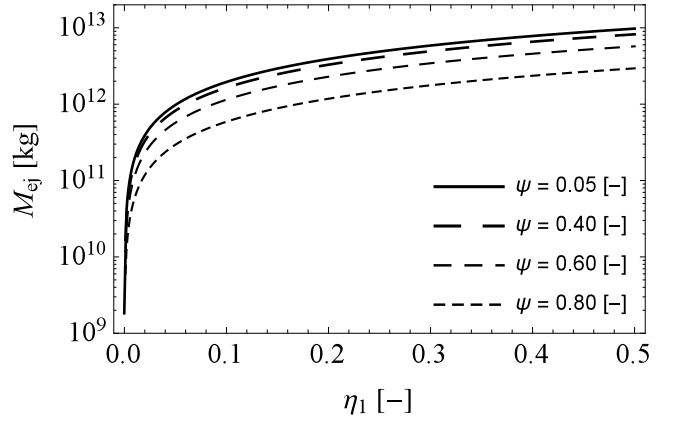


**Figure 3.** The amount of mass ejected during the outburst of comet 12P as a function of the fraction of the active surface during quiet sublimation. In the calculations, it was assumed that the scattering of incident sunlight occurs on porous dust agglomerates with an average radius of  $r_{\text{agg}} = 1$  mm, and the cometary activity was controlled by the sublimation of water ice. These calculations concern the outburst with the largest amplitude  $\Delta m = 5.00$  magnitude, which took place at a heliocentric distance of  $r_h = 2.59$  au.

of the cometary outburst, we quantified the number of particles according to Pogson’s law. The results of these calculations are shown in Figs.(4-5). Moreover, the type of ice responsible for the sublimation activity also influences the amplitude of the cometary outburst. To illustrate this effect, we calculated the outburst amplitude as a function of the ejected mass for two representative values of the active surface during the quiet sublimation phase. The results of these calculations are presented in Fig.6.

## 5 CLASSIFICATION OF COMETARY OUTBURSTS

A cometary outburst is primarily characterized by its brightness amplitude, which represents the magnitude of the observed brightness change. The amplitudes of cometary outbursts can range from subtle variations, as frequently observed in comet 67P/Churyumov–Gerasimenko, to dramatic phenomena like the spectacular October 2007 event of comet 17P/Holmes (Moreno et al. 2008; Montalto et al. 2008; Trigo-Rodríguez et al. 2008; Wesołowski and Gronkowski 2018).

Based on the amplitude of brightness change during an outburst, we propose a six-level classification scheme (Table 4). The classification categories span from minor glow variations to rare mega-outbursts, using amplitude as the defining metric. This framework enables systematic comparison and analysis of cometary activity across different comets and epochs.

In this study, we applied the classification to sixteen outbursts of comet 12P, finding that the majority of these events were classified as either Class F (six instances) or Class D (six instances), with the remaining two events identified as Class E. This distribution highlights the diverse nature of cometary activity and the prevalence of relatively low-intensity outbursts in the observed dataset.

## 6 DISCUSSION

Despite their sporadic nature, cometary outbursts offer unique opportunities to study the underlying processes shaping cometary activity and the formation of dust trails. In this study, we focused on

**Table 2.** The values of cometary parameters used in the numerical simulations.

Parameter	Value(s)	Reference
Radius of the cometary nucleus (km)	$R_N = 17 \pm 6$	(Ye et al. 2020)
Albedo of cometary nucleus (-)	$A_N=0.04$	Adopted value
Density of cometary agglomerate ( $\text{kg} \cdot \text{m}^{-3}$ )	$\rho_{\text{agg}}=875$	Adopted value
Density of cometary particles ( $\text{kg} \cdot \text{m}^{-3}$ )	$\rho_{\text{gr}}=2950$	(Davidsson and Skorov 2002)
Total area of the comet ( $\text{m}^2$ )	$S_N \approx 9.08 \cdot 10^8$	Adopted value
Emissivity (-)	$\epsilon = 0.9$	Adopted value
Radius of the coma (m)	$R_c=2.5 \cdot 10^8$	Adopted value
Index in the power law (-)	$q = 3.5$	Adopted value
Average radius of monomers (m)	$r = 1.67 \cdot 10^{-7}$	Adopted value
The upper limit of integration (m)	$r_{\text{max}} = 10^{-2}$	Adopted value
The lower limit of integration (m)	$r_{\text{max}} = 10^{-7}$	Adopted value
The thickness of the destroyed layer (m)	$h = 10$	Adopted value
Solar constant (for $d=1$ au) ( $\text{W} \cdot \text{m}^{-2}$ )	$S_{\odot}=1361.1$	(Gueymard 2018)
Constant $A_{\text{H}_2\text{O}}$ for water ice (Pa)	$A_{\text{H}_2\text{O}} = 3.56 \cdot 10^{12}$	(Priyalnik 2006)
Constant $B_{\text{H}_2\text{O}}$ for water ice (K)	$B_{\text{H}_2\text{O}} = 6141.667$	(Priyalnik 2006)
Latent heat of water ice sublimation ( $\text{J} \cdot \text{kg}^{-1}$ )	$H_{\text{H}_2\text{O}}=2.83 \cdot 10^6$	(Priyalnik 2006)
The molar mass of water ice ( $\text{g} \cdot \text{mol}^{-1}$ )	$m_{\text{H}_2\text{O}} = 18$	Adopted value
Constant $A_{\text{CO}_2}$ for carbon dioxide (Pa)	$A_{\text{CO}_2} = 107.9 \cdot 10^{10}$	(Priyalnik 2006)
Constant $B_{\text{CO}_2}$ for carbon dioxide (K)	$B_{\text{CO}_2} = 3148.0$	(Priyalnik 2006)
Latent heat of carbon dioxide sublimation ( $\text{J} \cdot \text{kg}^{-1}$ )	$H_{\text{CO}_2}=0.954 \cdot 10^6$	(Priyalnik 2006)
The molar mass of water ice ( $\text{g} \cdot \text{mol}^{-1}$ )	$m_{\text{CO}_2} = 44$	Adopted value
Constant $A_{\text{CO}}$ for carbon dioxide (Pa)	$A_{\text{CO}} = 0.1263 \cdot 10^{10}$	(Priyalnik 2006)
Constant $B_{\text{CO}}$ for carbon dioxide (K)	$B_{\text{CO}} = 764.16$	(Priyalnik 2006)
Latent heat of sublimation of carbon monoxide ( $\text{J} \cdot \text{kg}^{-1}$ )	$H_{\text{CO}}=0.227 \cdot 10^6$	(Priyalnik 2006)
The molar mass of water ice ( $\text{g} \cdot \text{mol}^{-1}$ )	$m_{\text{CO}} = 28$	Adopted value
The dust-to-gas mass ratio in the quiet sublimation phase (-)	$\gamma_1 = 1$	(Wesolowski and Potera 2024)
The dust-to-gas mass ratio in the outburst phase (-)	$\gamma_2 = 3$	(Wesolowski and Potera 2024)
Wavelength of electromagnetic solar radiation (m)	$\lambda = 0.50 \cdot 10^{-6}$	(Wesolowski et al. 2020)
The radius of the agglomerate (m)	$r_{\text{agg}} = 1 \cdot 10^{-3}$	Adopted value
Refractive index for cometary dust particles (-)	$n_{\text{dust}} = 1.60 + 0.005i$	(Wesolowski et al. 2020)
The scattering coefficient for cometary dust particles (-)	$Q_{\text{dust}}(r_{\text{agg}}) \approx 1$	(Wesolowski et al. 2020)

the well-documented outbursts of comet 12P, aiming to understand the mechanisms driving these phenomena, the mass of particles released, and their implications for cometary evolution. Through the development of a numerical model based on observational data, we aimed to estimate the mass ejected during these outbursts (Tab.3, and Fig.3). The measure of the total mass ejected is the number of particles coming from individual scattering cross-sections. According to our previous assumption, the largest contribution to the particle number comes from the scattering cross-section associated with the destruction of a fragment of the cometary nucleus (Figs.4-5). The nucleus challenge in such estimation lies in accurately determining the ice sublimation flux occurring through the porous structure of the cometary nucleus and accounting for the intricate interplay between sublimation activity, surface morphology, and thermodynamic conditions within the comet nucleus. By resolving the energy balance equation and employing relationships governing gas dynamics and sublimation processes, we elucidated the mechanisms contributing to mass ejection during outbursts.

Analyzing the effect of sublimation from individual ices on the amplitude of the outbursts reveals an upward trend in amplitude that is consistent with the increase in the mass ejected, for a fixed ejected mass (Fig.6). This trend corresponds to the number of particles on which incident sunlight is scattered. The outburst amplitude also depends on the active surface area, both during the quiet sublimation phase and the outburst, regardless of the type of ice that caused the outburst. From the obtained calculation results, it can be concluded that the outburst amplitude is larger when the fraction of the active

surface is smaller. This implies that the same amount of mass ejected after the destruction of a fragment of the nucleus surface is relatively larger compared to the mass contained in the coma for smaller values of the parameter  $\eta_1$ . For water-ice controlled sublimation, with an ejected mass of the order of  $10^{12}$  kg, the amplitude was  $\Delta m = -6.72$  magnitudes for the parameter  $\eta_1 = 10\%$  and  $\Delta m = -4.97$  magnitudes for the parameter  $\eta_1 = 50\%$ . In the case of  $\text{CO}_2$  ice controlled sublimation for the same value of mass ejected for the parameter  $\eta_1 = 10\%$  the amplitude value was  $\Delta m = -3.44$  magnitude and for the parameter  $\eta_1 = 50\%$  it was  $\Delta m = -1.86$  magnitude. Whereas for sublimation controlled by CO ice for the same value of mass ejected for the parameter  $\eta_1 = 10\%$  the value of the amplitude was equal to  $\Delta m = -1.86$  magnitude and for the parameter  $\eta_1 = 50\%$  it was  $\Delta m = -0.76$  magnitude. It is noteworthy that the sublimation flux directly influences the brightness change, with the highest flux observed for CO-ice sublimation and the lowest for water-ice sublimation. This suggests that a smaller sublimation flux leads to a larger amplitude for the same parameter  $\eta_1$  and the same amount of ejected mass. Our previous research supports this conclusion (Wesolowski 2023c).

The comparison of mass ejection between scenarios where sublimation activity is controlled by different types of ice, such as  $\text{H}_2\text{O}$  and  $\text{CO}_2$ , underscores the importance of understanding the composition and behavior of cometary nuclei. These findings not only enhance our understanding of individual cometary events but also have broader implications for our understanding of cometary evolution and the formation of dust trails. Analyzing the obtained results, we observe that as the porosity of the agglomerate increases, the value

**Table 3.** Values of thermodynamic parameters and ejected mass describing the outbursts of comet 12P. In the calculation of the ejected mass ( $M_{ej}$ ), a wide range of active surfaces in the quiet sublimation phase ( $\eta$  parameter) was taken into account ( $M_{ej1}$  corresponds to the active surface  $\eta = 10\%$ , and  $M_{ej2}$  corresponds to the active surface  $\eta = 50\%$ ). The values given in the last row of this table apply to situations when the sublimation of  $\text{CO}_2$  ice is responsible for the outburst(\*). The following symbols have been adopted in the table:  $r_h$  is the heliocentric distance at which the outburst occurred,  $\Delta m$  is the change in the cometary brightness,  $\psi$  is the porosity of the particle on which the incident sunlight is scattering,  $T$  is the temperature at the cometary surface,  $F(T)$  is the sublimation flux, and  $v_g$  is the gas velocity.

Outburst of date	$r_h$ [au]	$\Delta m$ [mag.]	$\psi$ [-]	$T$ [K]	$F(T)$ [ $\text{kg}\cdot\text{m}^{-2}\cdot\text{s}^{-1}$ ]	$v_g$ [ $\text{m}\cdot\text{s}^{-1}$ ]	$M_{ej1}$ [kg]	$M_{ej2}$ [kg]
2023/07/20.37±0.08 UT	3.89	5.50	0.40	189.294	$7.347\cdot 10^{-6}$	370.577	$5.596\cdot 10^{11}$	$2.798\cdot 10^{12}$
2023/07/20.37±0.08 UT	3.89	5.50	0.60	187.549	$8.187\cdot 10^{-6}$	368.865	$4.177\cdot 10^{11}$	$2.088\cdot 10^{12}$
2023/07/20.37±0.08 UT	3.89	5.50	0.80	186.291	$8.779\cdot 10^{-6}$	367.625	$2.247\cdot 10^{11}$	$1.123\cdot 10^{12}$
2023/09/04.00±0.60 UT	3.41	0.36	0.40	193.393	$1.446\cdot 10^{-5}$	374.5672	$2.773\cdot 10^9$	$1.386\cdot 10^{10}$
2023/09/04.00±0.60 UT	3.41	0.36	0.60	191.341	$1.551\cdot 10^{-5}$	372.575	$1.993\cdot 10^9$	$9.964\cdot 10^9$
2023/09/04.00±0.60 UT	3.41	0.36	0.80	189.887	$1.623\cdot 10^{-5}$	371.156	$1.047\cdot 10^9$	$5.235\cdot 10^9$
2023/09/23.87±0.02 UT	3.19	0.90	0.40	195.158	$1.918\cdot 10^{-5}$	376.273	$1.201\cdot 10^{10}$	$6.001\cdot 10^{10}$
2023/09/23.87±0.02 UT	3.19	0.90	0.60	192.992	$2.032\cdot 10^{-5}$	374.178	$8.527\cdot 10^9$	$4.262\cdot 10^{10}$
2023/09/23.87±0.02 UT	3.19	0.90	0.80	191.464	$2.110\cdot 10^{-5}$	372.694	$4.445\cdot 10^9$	$2.222\cdot 10^{10}$
2023/10/05.16±0.03 UT	3.06	5.00	0.40	196.185	$2.255\cdot 10^{-5}$	377.261	$1.063\cdot 10^{12}$	$5.317\cdot 10^{12}$
2023/10/05.16±0.03 UT	3.06	5.00	0.60	193.956	$2.374\cdot 10^{-5}$	375.112	$7.508\cdot 10^{11}$	$3.753\cdot 10^{12}$
2023/10/05.16±0.03 UT	3.06	5.00	0.80	192.388	$2.456\cdot 10^{-5}$	373.593	$3.898\cdot 10^{11}$	$1.949\cdot 10^{12}$
2023/10/22.52±0.21 UT	2.86	0.40	0.40	197.757	$2.881\cdot 10^{-5}$	378.770	$6.190\cdot 10^9$	$3.094\cdot 10^{10}$
2023/10/22.52±0.21 UT	2.86	0.40	0.60	195.439	$3.009\cdot 10^{-5}$	376.544	$4.334\cdot 10^9$	$2.167\cdot 10^{10}$
2023/10/22.52±0.21 UT	2.86	0.40	0.80	193.814	$3.095\cdot 10^{-5}$	374.975	$2.238\cdot 10^9$	$1.119\cdot 10^{10}$
2023/10/31.46±0.20 UT	2.76	2.90	0.40	198.545	$2.477\cdot 10^{-5}$	379.524	$2.089\cdot 10^{11}$	$1.044\cdot 10^{12}$
2023/10/31.46±0.20 UT	2.76	2.90	0.60	196.185	$3.253\cdot 10^{-5}$	377.262	$1.458\cdot 10^{11}$	$7.288\cdot 10^{11}$
2023/10/31.46±0.20 UT	2.76	2.90	0.80	194.533	$3.472\cdot 10^{-5}$	375.669	$7.512\cdot 10^{10}$	$3.755\cdot 10^{11}$
2023/11/01.40±0.15 UT	2.75	2.50	0.40	198.624	$3.293\cdot 10^{-5}$	379.599	$1.416\cdot 10^{11}$	$7.082\cdot 10^{11}$
2023/11/01.40±0.15 UT	2.75	2.50	0.60	196.261	$3.424\cdot 10^{-5}$	377.334	$9.879\cdot 10^{10}$	$4.939\cdot 10^{11}$
2023/11/01.40±0.15 UT	2.75	2.50	0.80	194.605	$3.512\cdot 10^{-5}$	375.739	$5.089\cdot 10^{10}$	$2.544\cdot 10^{11}$
2023/11/14.65±0.05 UT	2.59	5.00	0.40	199.897	$3.512\cdot 10^{-5}$	380.814	$1.867\cdot 10^{12}$	$9.332\cdot 10^{12}$
2023/11/14.65±0.05 UT	2.59	5.00	0.60	197.468	$3.646\cdot 10^{-5}$	378.494	$1.295\cdot 10^{12}$	$6.474\cdot 10^{12}$
2023/11/14.65±0.05 UT	2.59	5.00	0.80	195.771	$3.735\cdot 10^{-5}$	376.863	$6.649\cdot 10^{11}$	$3.324\cdot 10^{12}$
2023/11/30.60±0.02 UT	2.39	3.40	0.40	201.523	$5.100\cdot 10^{-5}$	382.359	$5.284\cdot 10^{11}$	$2.642\cdot 10^{12}$
2023/11/30.60±0.02 UT	2.39	3.40	0.60	199.017	$5.245\cdot 10^{-5}$	379.975	$3.645\cdot 10^{11}$	$1.823\cdot 10^{12}$
2023/11/30.60±0.02 UT	2.39	3.40	0.80	197.268	$5.343\cdot 10^{-5}$	378.301	$1.865\cdot 10^{11}$	$9.324\cdot 10^{11}$
2023/12/14.57±0.11 UT	2.22	1.65	0.40	202.951	$6.298\cdot 10^{-5}$	383.712	$1.066\cdot 10^{11}$	$5.332\cdot 10^{11}$
2023/12/14.57±0.11 UT	2.22	1.65	0.60	200.382	$6.449\cdot 10^{-5}$	381.275	$7.328\cdot 10^{10}$	$3.664\cdot 10^{11}$
2023/12/14.57±0.11 UT	2.22	1.65	0.80	198.591	$6.552\cdot 10^{-5}$	379.568	$3.739\cdot 10^{10}$	$1.869\cdot 10^{11}$
2024/01/18.40±0.05 UT	1.77	1.90	0.40	207.082	$1.140\cdot 10^{-4}$	387.597	$2.542\cdot 10^{11}$	$1.271\cdot 10^{12}$
2024/01/18.40±0.05 UT	1.77	1.90	0.60	204.345	$1.157\cdot 10^{-4}$	385.027	$1.732\cdot 10^{11}$	$8.661\cdot 10^{11}$
2024/01/18.40±0.05 UT	1.77	1.90	0.80	202.443	$1.168\cdot 10^{-4}$	383.231	$8.788\cdot 10^{10}$	$4.393\cdot 10^{11}$
2024/02/02.95±0.75 UT	1.57	0.60	0.40	209.169	$1.525\cdot 10^{-4}$	389.546	$5.273\cdot 10^{10}$	$2.636\cdot 10^{11}$
2024/02/02.95±0.75 UT	1.57	0.60	0.60	206.355	$1.543\cdot 10^{-4}$	386.917	$3.581\cdot 10^{10}$	$1.790\cdot 10^{11}$
2024/02/02.95±0.75 UT	1.57	0.60	0.80	204.401	$1.555\cdot 10^{-4}$	385.080	$1.813\cdot 10^{10}$	$9.066\cdot 10^{10}$
2024/02/29.40±0.20 UT	1.21	0.70	0.40	213.595	$2.773\cdot 10^{-4}$	393.645	$1.164\cdot 10^{11}$	$5.820\cdot 10^{11}$
2024/02/29.40±0.20 UT	1.21	0.70	0.60	210.627	$2.793\cdot 10^{-4}$	390.901	$7.872\cdot 10^{10}$	$3.936\cdot 10^{11}$
2024/02/29.40±0.20 UT	1.21	0.70	0.80	208.569	$2.807\cdot 10^{-4}$	388.986	$3.974\cdot 10^{10}$	$1.987\cdot 10^{11}$
2024/04/02.95±0.10 UT	0.85	0.90	0.40	219.542	$5.808\cdot 10^{-4}$	399.088	$3.516\cdot 10^{11}$	$1.758\cdot 10^{12}$
2024/04/02.95±0.10 UT	0.85	0.90	0.60	216.381	$5.961\cdot 10^{-4}$	396.204	$2.371\cdot 10^{11}$	$1.185\cdot 10^{12}$
2024/04/02.95±0.10 UT	0.85	0.90	0.80	214.191	$5.985\cdot 10^{-4}$	394.194	$1.194\cdot 10^{11}$	$5.972\cdot 10^{11}$
2024/06/10	1.20	2.20	0.40	213.734	$2.694\cdot 10^{-4}$	393.774	$8.581\cdot 10^{11}$	$4.291\cdot 10^{12}$
2024/06/10	1.20	2.20	0.60	210.762	$2.825\cdot 10^{-4}$	391.026	$5.802\cdot 10^{11}$	$2.901\cdot 10^{12}$
2024/06/10	1.20	2.20	0.80	208.701	$2.859\cdot 10^{-4}$	389.109	$2.929\cdot 10^{11}$	$1.464\cdot 10^{12}$
2024/08/30.39-31.02 UT	2.26	0.96	0.40	202.611	$5.990\cdot 10^{-5}$	383.389	$4.048\cdot 10^{10}$	$2.024\cdot 10^{11}$
2024/08/30.39-31.02 UT	2.26	0.96	0.60	200.056	$6.140\cdot 10^{-5}$	380.965	$2.784\cdot 10^{10}$	$1.392\cdot 10^{11}$
2024/08/30.39-31.02 UT	2.26	0.96	0.80	198.275	$6.242\cdot 10^{-5}$	379.265	$1.421\cdot 10^{10}$	$7.107\cdot 10^{10}$
2023/10/05.16±0.03 UT(*)	3.06	5.00	0.40	108.411	$1.388\cdot 10^{-4}$	179.373	$1.376\cdot 10^{13}$	$6.884\cdot 10^{13}$
2023/10/05.16±0.03 UT(*)	3.06	5.00	0.60	106.903	$1.392\cdot 10^{-4}$	178.121	$9.270\cdot 10^{12}$	$4.635\cdot 10^{13}$
2023/10/05.16±0.03 UT(*)	3.06	5.00	0.80	105.858	$1.395\cdot 10^{-4}$	177.248	$4.667\cdot 10^{12}$	$2.334\cdot 10^{13}$

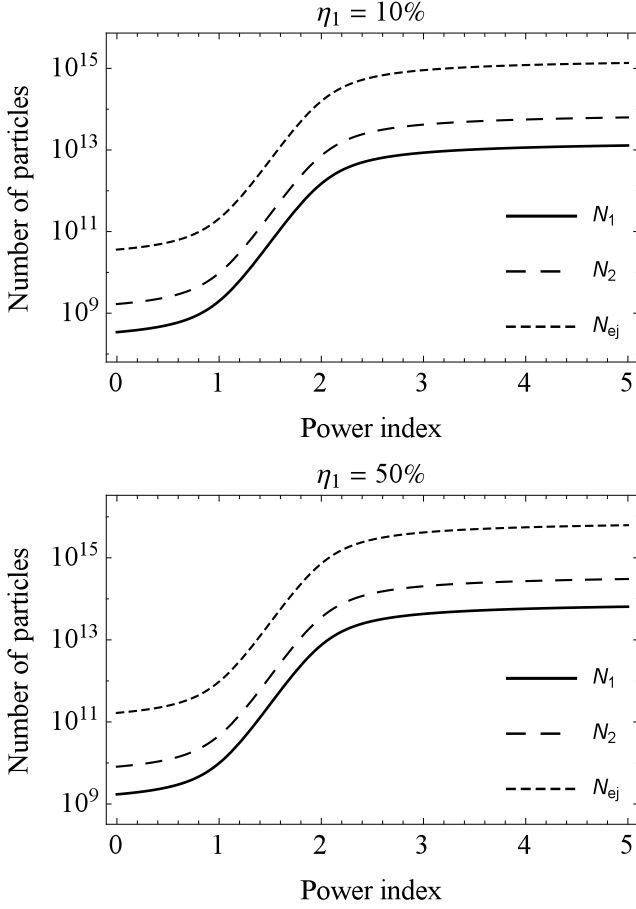


**Figure 4.** The number of particles on which incident sunlight is scattered as a function of the power index  $q$ . The considerations took into account that the cometary outburst amplitude was  $\Delta m = 5.00$  magnitude, and the outburst took place at a distance of  $r_h = 2.59$  au on 2023/07/20.37 $\pm$ 0.08 UT. The number of these particles was calculated per unit area. In addition, the calculations take into account two active surfaces in the quiet sublimation phase, the upper panel concerns the surface  $\eta_1 = 10\%$ , and the lower panel concerns the surface  $\eta_1 = 50\%$ . The calculations assume that the incident sunlight is scattered on dense dust particles with a porosity of  $\psi = 0.05$ . The symbols used mean:  $N_1$  is the number of particles lifted into the coma during the quiet sublimation,  $N_2$  is the number of particles carried into the coma during the cometary outburst,  $N_{ej}$  is the number of particles created as a result of the destruction of a fragment of the cometary nucleus.

**Table 4.** A six-level classification scheme of cometary outbursts based on observational data.

Class	Title	Amplitude [magnitude]
A	Mega-outburst	$12 \leq \Delta m \leq 14$
B	Strong outburst	$10 \leq \Delta m < 12$
C	Intense outburst	$6 \leq \Delta m < 10$
D	Typical outburst	$2 \leq \Delta m < 6$
E	Mini-outburst	$1 \leq \Delta m < 2$
F	Glow variation	$0.01 \leq \Delta m < 1$

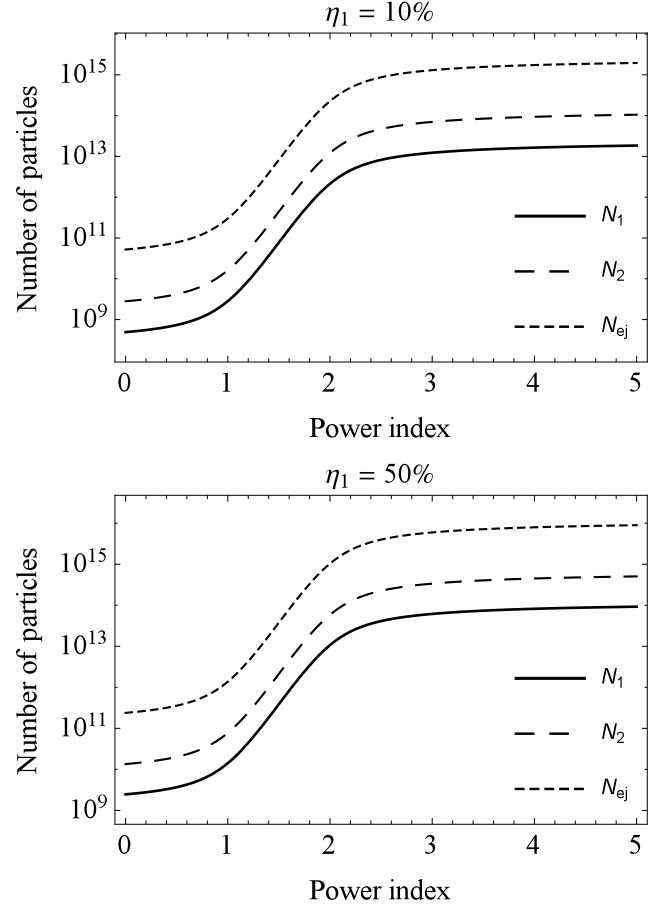


**Figure 5.** The number of particles on which incident sunlight is scattered as a function of the power index  $q$ . This situation is analogous to that shown in Fig.(4), but the scattering of incident sunlight takes place on dust particles with porosity  $\psi = 0.8$ . The remaining symbols are analogous to those shown in Fig.(4).

of the mass ejected for a given outburst amplitude is lower, which is a consequence of the density of the agglomerates. In the case of  $H_2O$  ice, the upper limit of the mass ejected for the parameter  $\eta=50\%$  is of the order  $10^{12}$  kg. However, in the case of an outburst controlled by the sublimation of  $CO_2$  ice, the upper limit of the mass ejected for the parameter  $\eta=50\%$  is of the order  $10^{13}$  kg. A comparison of the amount of mass ejected depending on the type of ice responsible for the initiation of the outburst is shown in Fig.(7). The calculated sublimation flux and gas velocity values provide quantitative measures of mass loss and gas production during outbursts, contributing to our understanding of the mechanisms driving cometary activity and the subsequent evolution of the coma and resulting dust trail. Differential effects of radiation pressure on dust particles lead to changes in their orbital parameters, resulting in the formation of enduring dust trails observable in subsequent comet revolutions. In the context of visual observations of comets, and especially cometary dust trails, the key parameter is the quality of the night sky, i.e., the level of its pollution with artificial light (Wesolowski 2019, 2023a). Despite the increasing level of pollution of the night sky with artificial light, comets are an example of celestial bodies that, with a strong outburst, can be visually observed even with the naked eye (Wesolowski 2019), such as the outburst of comet 17P/Holmes in 2007 (Trigo-Rodríguez et al.

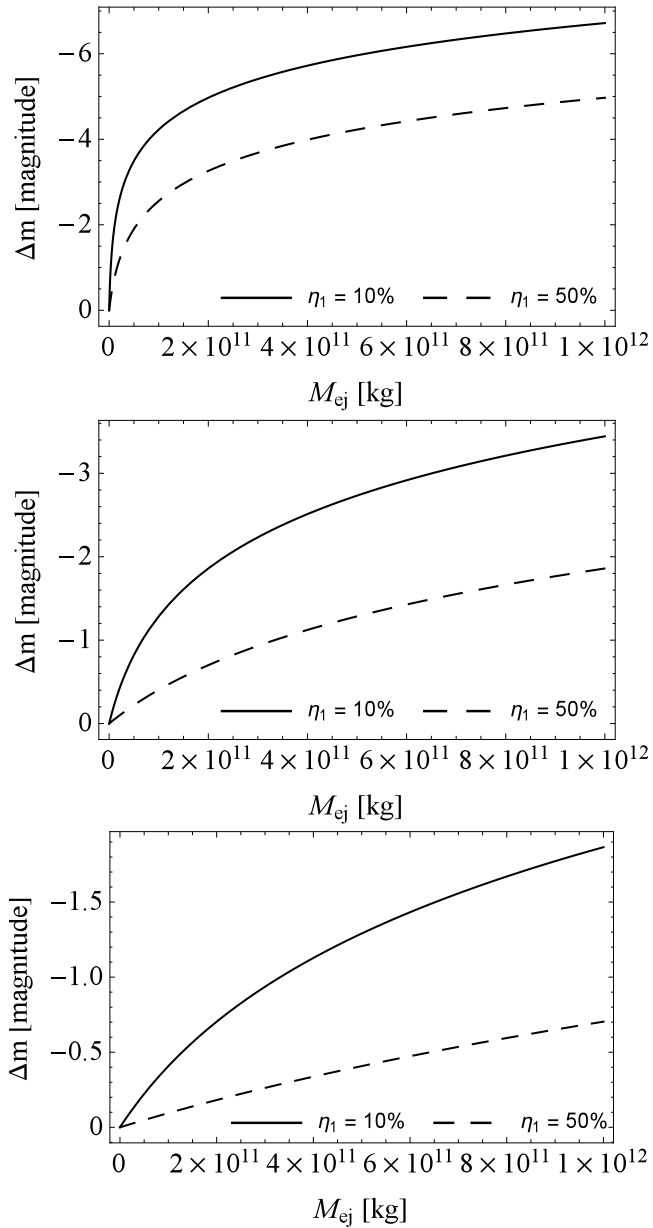


**Figure 6.** The change in comet brightness as a function of the ejected mass for two exemplary values of the active surface area in the quiescent phase of sublimation. The calculations assume that the scattering of incident sunlight occurs on porous dust agglomerates ( $\psi = 0.7$ ) and that the outburst occurred at a distance of  $r_h = 3.89$  au. Furthermore, the upper panel is associated with sublimation controlled by water ice, the middle panel is associated with sublimation controlled by carbon dioxide ice, and the lower panel is associated with sublimation controlled by carbon monoxide ice.

2008; Gritsevich et al. 2022) and visually comparable outbursts of 12P studied in this paper.

## 7 CONCLUSIONS

This study provides valuable insights into the physical properties and dynamic behavior of comet 12P during its outburst events experienced during the last return. The estimated characteristics and albedo of the nucleus suggest a moderately sized object with typical

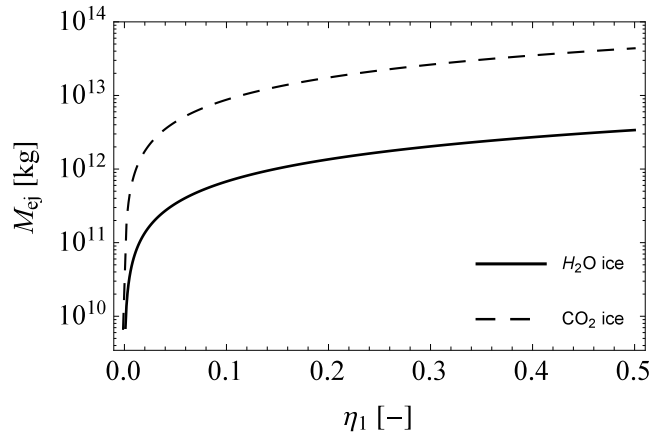


**Figure 7.** Comparison of the amount of mass ejected during the outburst of comet 12P for a distance of  $r_h = 3.06$  au as a function of the active surface ( $\eta_1$ ). Furthermore, it was assumed that the sublimation activity is controlled by  $H_2O$  ice or  $CO_2$  ice.

reflective characteristics for a comet. The recorded outburst dates, heliocentric distances, and amplitudes reveal a pattern of periodic activity, influenced by the changes in the comet’s internal structure and variations in solar heating. Thermal properties such as emissivity and coma radius indicate significant thermal activity driven by the sublimation of volatile materials. The porosity and temperature values play crucial roles in controlling sublimation rates and the extent of outburst events. The sublimation flux and gas velocity calculations offer quantitative measures of mass loss and gas production, enhancing our understanding of cometary activity and subsequent coma and dust trail evolution. The comparison between  $H_2O$  and  $CO_2$  ice-controlled sublimation scenarios show that  $CO_2$  sublimation results in a higher mass ejection, underscoring the importance of understanding the composition and behavior of cometary nuclei in predicting outburst magnitudes. Increasing agglomerate porosity reduces the mass ejected for a given outburst amplitude due to the lower density of the agglomerates. The differential effects of radiation pressure on dust particles released in these outbursts contribute to the creation of enduring dust trails observable in subsequent comet revolutions. Thus, our study not only deepens our understanding of individual cometary outburst events but also provides broader insights crucial for constraining the formation and long-term evolution of meteoroid swarms.

## ACKNOWLEDGEMENTS

We gratefully acknowledge the many collaborators with whom we exchanged observations and engaged in discussions, especially T. Prystavski, J. Ryske, I. Pérez-García, M. Nissinen, J. M. Trigo-Rodríguez, E. Peña-Asensio, I. Boaca, M. Husárik, O. Ivanova, A. Sánchez, and J. M. Llenas. We express our gratitude to the Finnish Geospatial Research Institute and the Academy of Finland for supporting the project no. 325806 (PlanetS), which facilitated the relevant observations and development of the methods presented in this paper. The program of development within Priority-2030 is acknowledged for supporting the research at UrFU. This work received support from the Centre for Innovation and Transfer of Natural Sciences and Engineering Knowledge, University of Rzeszów, Poland (RPPK.01.03.00-18-001/10-00), the Spanish Ministry of Science, Innovation and Universities projects No PID2023-151905OB-I00 and



PID2020-118491GB-I00, Junta de Andalucía grant P20\_010168, and the Centro de Excelencia Severo Ochoa grant CEX2021-001131-S funded by MCIN/AEI/10.13039/501100011033.

## DATA AVAILABILITY

The data underlying this study are included within the article.

## REFERENCES

- Belousov, D. V., Pavlov, A. K., 2024a. Cometary outbursts in the Oort cloud. *Icarus* 415, 116066. DOI: 10.1016/j.icarus.2024.116066
- Belousov, D. V., Pavlov, A. K., 2024b. Non-gravitational Mechanism of Comets' Ejection from the Oort Cloud Due to Cometary Outbursts. *Solar System Research* 57, 629-635. DOI: 10.1134/S0038094623060023
- Borderes-Motta, G., Gritsevich, M., Kastinen, D., Kero, J., 2024. On the Journey of the Meteoroids Ejected from 12P/Pons-Brooks During the Outbursts of 2023–2024. 86th Annual Meeting of the Meteoritical Society Meeting, held 28 July-2 August 2, 2024 in Brussels, Belgium. LPI Contribution No. 3036, 2024, id.6270.
- Castro-Tirado, A. J., Soldán, J., Bernas, M., Páta, P., Rezek, T., Hudec, R., Mateo Sanguino, T. J., de La Morena, B., Berná, J. A., Rodríguez, J., Peña, A., Gorosabel, J., Más-Hesse, J. M., & Giménez, A. 1999. The Burst Observer and Optical Transient Exploring System (BOOTES). *Astronomy and Astrophysics Supplement* 138, 583–585. DOI: 10.1051/aas:1999362
- Castro-Tirado, A. J., 2023. Tracking transients night and day. *Nature Astronomy* 7, 1136-1136. DOI: 10.1038/s41550-023-02075-w
- Crifo, J.-F., Loukianov, G. A., Rodionov, A. V., Zakharov, V. V., 2005. Direct Monte Carlo and multifluid modeling of the circumnuclear dust coma. Spherical grain dynamics revisited. *Icarus* 176, 192-219. DOI: 10.1016/j.icarus.2005.01.003
- Christou, A. A., 2010. Annual meteor showers at Venus and Mars: lessons from the Earth. *MNRAS* 402, 2759-2770. DOI: 10.1111/j.1365-2966.2009.16097.x
- Christou, A. A., Gritsevich, M., 2024. Feasibility of meteor surveying from a Venus orbiter. *Icarus* 417, 116116. DOI: 10.1016/j.icarus.2024.116116
- Davidsson, B. J. R., Skorov, Y. V., 2002. On the Light-Absorbing Surface Layer of Cometary Nuclei. II. Thermal Modeling. *Icarus* 159, 239-258. DOI: 10.1006/icar.2002.6912
- Gicquel, A., Vincent, J.-B., Agarwal, J., A'Hearn, M. F., Bertini, I., et al. 2016. *MNRAS* 462, S57-S66. DOI: 10.1093/mnras/stw2117
- Gronkowski, P., Wesołowski, M., 2015. A model of cometary outbursts: a new simple approach to the classical question. *MNRAS* 451, 3068-3077. DOI: 10.1093/mnras/stv1122
- Gritsevich, M., Nissinen, M., Oksanen, A., Suomela, J., Silber, E. A., 2022. Evolution of the dust trail of comet 17P/Holmes. *MNRAS* 513, 2201-2214. DOI: 10.1093/mnras/stac822
- Gritsevich, M., Nissinen, M., Ryske, J., et al. 2025a. *Rev. Mex. Astron. Astrof. Conf. Ser.*, in press
- Gritsevich, M., Wesołowski, M., Prystavski, T., Castro-Tirado, A. J., 2025b. Astronomical Observations of Comet 12P/Pons-Brooks: From Initial Activity in June 2023 to Post-Perihelion Outbursts in 2024. *Zenodo*. DOI: 10.5281/zenodo.14739570
- Gueymard, C. A., 2018. A reevaluation of the solar constant based on a 42-year total solar irradiance time series and a reconciliation of spaceborne observations. *Sol. Energy* 168, 2-9. DOI: 10.1016/j.solener.2018.04.001
- Guliev, A. S., Poladova, U. D., Guliev, R. A., 2022. On the Nature of Impacts Causing Cometary Outbursts. *Solar System Research* 56, 233-240. DOI: 10.1134/S0038094622040050
- Hughes, D. W., 1990. Cometary outbursts - A review. *Royal Astronomical Society, Quarterly Journal* 31, 69-94.
- Hu, Y.-D., Fernández-García, E., Caballero-García, M. D., Pérez-García, I., Carrasco-García, I. M., Castellón, A., Pérez del Pulgar, C., Reina Terol, A. J., and Castro-Tirado, A. J. 2023. The Burst Observer and Optical Transient Exploring System in the Multi-Messenger Astronomy Era. *Frontiers in Astronomy and Space Sciences* 10: 952887. <https://doi.org/10.3389/fspas.2023.952887>.
- Knight, M. M., Skiff, B. A., Schleicher, D. G., Spiro, L. G., Fernald, I. C., Guan, B. Y., Lininger, L. J., Larsen, J. A., 2024. Rotation period of comet 12P/Pons-Brooks from CN coma morphology. *The Astronomer's Telegram*, No. 16508
- Kossacki, K. J., Wesołowski, M., Skora, G., Staszkievicz, K., 2022. Comets, sliding of surface dust II. *Icarus* 379, 114946. DOI: 10.1016/j.icarus.2022.114946
- Lyytinen, E., Nissinen, M., Lehto, H. J., 2023. Comet 17P/Holmes: originally widely spreading dust particles from the 2007 explosion converge into an observable dust trail near the common nodes of the meteoroids' orbits. *Journal of the International Meteor Organization* 41, 77-83.
- Miles, R., 2016a. Discrete sources of cryovolcanism on the nucleus of Comet 29P/Schwassmann-Wachmann and their origin. *Icarus* 272, 387-413. DOI: 10.1016/j.icarus.2015.11.011
- Miles, R., 2016b. Heat of solution: A new source of thermal energy in the subsurface of cometary nuclei and the gas-exsolution mechanism driving outbursts of Comet 29P/Schwassmann-Wachmann and other comets. *Icarus* 272, 356-386. DOI: 10.1016/j.icarus.2015.12.053
- Montalto, M., Riffeser, A., Hopp, U., Wilke, S., Carraro, G., 2008. The comet 17P/Holmes 2007 outburst: the early motion of the outburst material. *A&A* 479, L45 - L49. DOI: 10.1051/0004-6361:20079130
- Moreno, F., Ortiz, J. L., Santos-Sanz, P., et al., 2008. A Model of the Early Evolution of the 2007 Outburst of Comet 17P/Holmes. *ApJ* 677, L63. DOI: 10.1086/587838
- Müller, D. R., Altwegg, K., Berthelier, J.-J., Combi, M. R., De Keyser, J., et al. 2024. Deciphering cometary outbursts: linking gas composition changes to trigger mechanisms. *Monthly Notices of the Royal Astronomical Society* 529, 2763-2776. DOI: 10.1093/mnras/stae622
- Prialnik, D., Brosch, N., Ianovici, D., 1995. Modelling the activity of 2060 Chiron. *MNRAS* 276, 1148-1154. DOI: 10.1093/mnras/276.4.1148
- Prialnik, D., 2006. What makes comets active? Asteroids, Comets, Meteors, Proceedings of the 229th IAU Symposium, Cambridge Univ. Press, 153-170.
- Prystavski, T., Gritsevich, M., Ryske, J., Nissinen, M., 2024. Dust Production Dynamics of the Comet 12P/Pons-Brooks. 55th Lunar and Planetary Science Conference, 3040, 2385.
- Ryske, J., Gritsevich, M., Nissinen, M., Perez-Garcia, I., & Castro-Tirado, A. J., 2023. Expansion rates of the comet 12P/Pons-Brooks, currently in outburst. *The Astronomer's Telegram*, 2023, 16343.
- Skiff, B., 2018. Outburst of comet 174/Echeclus. *J. Br. Astron. Assoc.* 128, 51.
- Thomas, N., Davidsson, B., El-Maarry, M. R., Fornasier, S., Giacomini, L., et al. 2015. Redistribution of particles across the nucleus of comet 67P/Churyumov-Gerasimenko. *Astronomy & Astrophysics* 583, A17. DOI: 10.1051/0004-6361/201526049
- Trigo-Rodríguez, J. M., Davidsson, B., Montanes-Rodríguez, P., Sanchez, A., Troughton, B., 2008. All-Sky Cameras Detection and Telescope Follow-Up of the 17P/Holmes Outburst. 39th Lunar and Planetary Science Conference, (Lunar and Planetary Science XXXIX), held March 10-14, 2008 in League City, Texas. LPI Contribution No. 1391., p.1627
- Trigo-Rodríguez, J. M., Sanchez, A., Llenas, J. M., Gritsevich, M., 2024. Photometric Follow-Up of Halley-Type Comet 12P/Pons-Brooks: Outbursts Experienced During the Pre-Perihelion Approach. 55th Lunar and Planetary Science Conference, held 11-15 March, 2024 at The Woodlands, Texas/Virtual. LPI Contribution No. 3040, id.1363
- Tomko, D., Neslušan, L., 2016. Meteoroid stream of 12P/Pons-Brooks, December  $\kappa$ -Draconids, and Northern June Aquilids. *Astronomy & Astrophysics* 592, A107. DOI: 10.1051/0004-6361/201628404
- Vincent, J.-B., A'Hearn, M. F., Lin, Z.-Y., El-Maarry, M. R., Pajola, M., et al. 2016. Summer fireworks on comet 67P. *MNRAS* 462, S184-S194. DOI: 10.1093/mnras/stw2409
- Wesołowski, M., Gronkowski, P., 2018. A new method for determining the mass ejected during the cometary outburst – Application to the Jupiter-family comets. *New Astronomy* 62, 55–61. DOI: 10.1016/j.newast.2018.01.006

- Wesołowski, M., 2019. Impact of light pollution on the visibility of astronomical objects in medium-sized cities in Central Europe on the example of the city of Rzeszów, Poland. *Journal of Astrophysics and Astronomy* 40, 20. DOI: 10.1007/s12036-019-9586-1
- Wesołowski, M., Gronkowski, P., Tralle, I., 2020. Outbursts of comets at large heliocentric distances: concise review and numerical simulations of brightness jumps. *Planetary & Space Science* 184, 104867. DOI: 10.1016/j.pss.2020.104867
- Wesołowski, M., 2021. The influence of the size of ice-dust particles on the amplitude of the change in the brightness of a comet caused by an outburst. *MNRAS* 505, 3525-3536. DOI: 10.1093/mnras/stab1418
- Wesołowski, M., 2022a. The rise time of the change of cometary brightness during its outburst. *Icarus* 375, 114847. DOI: 10.1016/j.icarus.2021.114847
- Wesołowski, M., Gronkowski, P., Kossacki, K. J., 2022b. The influence of the porosity of dust particles on the amplitude of the change in the brightness of a comet. *MNRAS* 517, 4950-4958 DOI: 10.1093/mnras/stac2967
- Wesołowski, M., 2023a. The increase in the surface brightness of the night sky and its importance in visual astronomical observations. *Scientific Reports* 13, 17091. DOI: 10.1038/s41598-023-44423-w
- Wesołowski, M., 2023b. Modelling of the processes of dunes formation on the surface of comet 67P/Churyumov-Gerasimenko. *MNRAS* 521, 1570-1577. DOI: 10.1093/mnras/stad658
- Wesołowski, M., 2023c. Influence of Water Ice Sublimation Flux on the Change of Cometary Brightness during the Outburst. *Acta Astronomica* 73, 243-258. DOI: 10.32023/0001-5237/73.3.4
- Wesołowski, M., 2024. Ejection of porous dust-ice agglomerates from the surface of the cometary nucleus. *Icarus* 411, 115937. DOI: 10.1016/j.icarus.2023.115937
- Wesołowski, M., Potera, P., 2024. Determination of bolometric albedo based on spectroscopic measurements for selected dust analogues and its impact on the change of cometary brightness during its outburst. *Astronomy & Astrophysics* 686, A248. DOI: 10.1051/0004-6361/202449573
- West, R. M., Hainaut, O., Smette, A., 1991. Post-perihelion observations of P/Halley. III - an outburst at R = 14.3 au. *Astronomy and Astrophysics* 246, L77-L80.
- Ye, Q., Farnham, T. L., Knight, M. M., Holt, C. E., Feaga, L. M., 2020. Recovery of Returning Halley-type Comet 12P/Pons-Brooks with the Lowell Discovery Telescope. *Research Notes of the AAS* 4, 101. DOI: 10.3847/2515-5172/aba2d1
- Ye, Q., Vaubaillon, J., 2022. The 2022 encounter of the outburst material from comet 73P/Schwassmann-Wachmann 3. *Monthly Notices of the Royal Astronomical Society: Letters* 515, L45-L49. DOI: 10.1093/mnrasl/slac070
- Yeomans, D. K., 1986. The intermediate comets and nongravitational effects. *Astronomical Journal* 91, 971-973. DOI: 10.1086/114073
- Usher, H., Milles, R., Pérez Redondo, J.M., Wooding, B., Kelley, M. S. P. et al. 2023. Large outburst comet 12P/Pons-Brooks, ATel 16270.

## APPENDIX A: EJECTION OF POROUS DUST AGGLOMERATES IN THE QUIET SUBLIMATION PHASE

An additional mechanism responsible for ejecting porous agglomerates into the coma is quiet sublimation, which peaks near perihelion. To comprehensively describe the activity of comet 12P, we calculated the minimum and maximum radii of porous agglomerates ejected into the coma. To simplify our considerations, we assumed that all the energy that was absorbed by the nucleus of comet 12P was used for the sublimation of water ice. To accurately model the emission of porous agglomerates during quiet sublimation, we considered two scenarios. The first scenario involves agglomerates on the nucleus surface that are not bound to their surroundings, while the second scenario involves agglomerates that are bound to their surroundings. A detailed discussion of these scenarios was recently presented in (Wesołowski 2024). Then the relationships for the minimum and

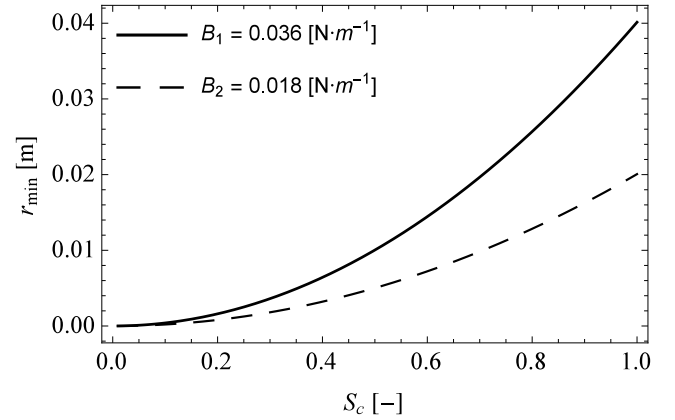


**Figure A.1.** The minimum radius of a particle that can be lifted into the coma from the surface of the cometary nucleus as a function of the degree of particle cleanliness ( $S_c$ ). The calculations were performed assuming that comet 12P is at perihelion and the sublimation of water ice controls its activity.

maximum particle radii are provided by Eqs.(A1-A2):

$$r_{\min} = \frac{B_i S_c^2}{0.5 C_D \pi v_g F_i}, \quad (\text{A1})$$

and

$$r_{\max} = \frac{3 C_D v_g F_i}{8 \rho_{gr} (1 - \psi) (g_c - 4\pi^2 R_N P^{-2})}. \quad (\text{A2})$$

In Eqs.(A1-A2), the individual symbols mean:  $B_i$  is a parameter related to the cohesion force ( $B_1 = 0.036 \text{ N}\cdot\text{m}^{-1}$  (Kossacki et al. 2022),  $B_2 = 0.018 \text{ N}\cdot\text{m}^{-1}$  (Thomas et al. 2015)),  $S_c$  describes the degree of particle cleanliness,  $C_D$  is the modified free-molecular drag coefficient for the spherical body ( $C_D = 2$ ),  $v_g$  is the gas velocity which is calculated based on the Eq.(8),  $F_i$  is the sublimation flux which is calculated based on the Eqs.(9),  $\rho_{gr}$  is the density of particles,  $g_c$  is the gravitational acceleration of the cometary nucleus ( $g_c = 2.38 \cdot 10^{-3}$ ), and  $P$  is the period of its rotation ( $P = 57 \pm 1 \text{ h}$ , Knight et al. (2024)). Note that in Eq.(A2), to simplify it, the influence from solar radiation pressure has been omitted, which is discussed in detail in (Crifo et al. 2005). The results of the particle radius calculations are shown in Figs.(A.1-A.2).

Analyzing the results presented in this paper, it can be noted that cometary outbursts, due to their energetic nature, are responsible for the occurrence of small grains of primary matter in the coma. In contrast, sublimation activity is responsible for the emission of much larger porous dust agglomerates.

This paper has been typeset from a  $\text{\TeX}/\text{\LaTeX}$  file prepared by the author.

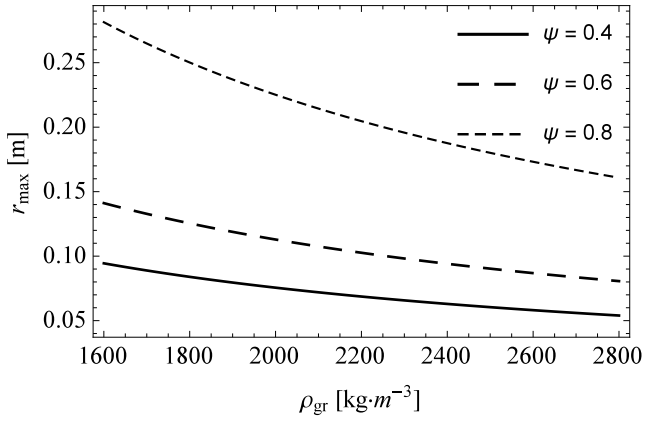


**Figure A.2.** The maximum radius of dust agglomerates that can be lifted into the coma from the surface of the cometary nucleus as a function of the particle density ( $\rho_{\text{gr}}$ ). The calculations are based on the same assumptions as in Fig.(A.1).